Title

Time-coded neurotransmitter release at excitatory and inhibitory synapses

Journal

Proceedings of the National Academy of Sciences of the United States of America, 113(8)

ISSN

0027-8424

Authors

Rodrigues, Serafim
Desroches, Mathieu
Krupa, Martin
et al.

Publication Date

2016-02-23

DOI

10.1073/pnas.1525591113

Peer reviewed

Time-coded neurotransmitter release at excitatory and inhibitory synapses

Serafim Rodrigues[a,1], Mathieu Desroches[b,1], Martin Krupa[b,1], Jesus M. Cortes[c,d], Terrence J. Sejnowski[e,f,g,2], and Afia B. Ali[h,1]

[a]School of Computing and Mathematics, Plymouth University, Plymouth PL4 8AA, United Kingdom; [b]Inria Sophia Antipolis Mediterranee Research Centre, MathNeuro Team, 06902 Sophia Antipolis cedex, France; [c]Biocruces Health Research Institute, Cruces University Hospital, 48903 Barakaldo, Bizkaia, Spain; [d]Departamento de Biologia Celular e Histologia, University of the Basque Country, 48940 Leioa, Bizkaia, Spain; [e]The Computational Neurobiology Laboratory, Salk Institute, La Jolla, CA 92037; [f]Howard Hughes Medical Institute, Salk Institute, La Jolla, CA 92037; [g]Division of Biological Science, University of California, San Diego, La Jolla, CA 92093; and [h]UCL School of Pharmacy, Department of Pharmacology, University College London, London WC1N 1AX, United Kingdom

Contributed by Terrence J. Sejnowski, December 30, 2015 (sent for review January 1, 2015; reviewed by Antoni Guillamon and Misha Tsodyks)

Communication between neurons at chemical synapses is regulated by hundreds of different proteins that control the release of neurotransmitter that is packaged in vesicles, transported to an active zone, and released when an input spike occurs. Neurotransmitter can also be released asynchronously, that is, after a delay following the spike, or spontaneously in the absence of a stimulus. The mechanisms underlying asynchronous and spontaneous neurotransmitter release remain elusive. Here, we describe a model of the exocytotic cycle of vesicles at excitatory and inhibitory synapses that accounts for all modes of vesicle release as well as short-term synaptic plasticity (STSP). For asynchronous release, the model predicts a delayed inertial protein unbinding associated with the SNARE complex assembly immediately after vesicle priming. Experiments are proposed to test the model's molecular predictions for differential exocytosis. The simplicity of the model will also facilitate large-scale simulations of neural circuits.

SM complex | exocytotic-endocytotic cycle | short-term synaptic plasticity | SNARE complex | asynchronous neurotransmitter release

Molecular and electrophysiological data have revealed differences in the regulation of presynaptic exocytotic machinery, giving rise to multiple forms of neurotransmitter release: synchronous release promptly after stimulation, delayed asynchronous release, and spontaneous release. Synchronous release is induced by rapid calcium influx and, subsequently, calcium-mediated membrane fusion (1). Asynchronous release occurs only under certain conditions (1, 2). Finally, spontaneous mini-releases occur in the absence of action potentials (2).

Two distinct mechanisms have been proposed to explain the various modes of exocytosis. One view suggests distinct signaling pathways and possibly independent vesicle pools (3, 4). The second and more parsimonious view argues that the three modes of release share key mechanisms for exocytosis, specifically, the canonical fusion machinery that operates by means of the interaction between the SNARE attachment protein receptor proteins and Sec1/Munc18 (SM) proteins (5–10) (Fig. 1). The SNARE proteins syntaxin, 25-kDa synaptosome-associated protein (SNAP-25), and vesicle-associated membrane protein (VAMP2; also called synaptobrevin 2), localized on the plasma membrane and the synaptic vesicle, bind to form a tight protein complex, bridging the membranes to fuse.

The canonical building block forms a substrate from which the three release modes differentially specialize with additional regulatory mechanisms and specific Ca^{2+} sources(s) and sensor(s) that trigger the exocytosis cycle. Calcium sensors for synchronous release have been identified as synaptotagmin (e.g., Syt1, Syt2, Syt9). In contrast, the biomolecular processes generating asynchronous and spontaneous release remain unclear and controversial. However, experiments suggest multiple mechanistically distinct forms of asynchronous release operating at any given synapse, and these forms have been associated, for example, with vesicle-associated membrane protein 4 (VAMP4), synaptotagmin (Syt7), double C2 domain protein (Doc2) (still controversial), Rab3-interacting molecules (RIM) proteins, phosphoprotein isoforms synapsin (Syn I and Syn II), and endocannabinoids (eCBs) (11–16). These views are still being debated due to fragmentary and conflicting data (reviewed in 17). In addition, synaptic molecular machinery regulates short-term synaptic plasticity (STSP); however, it is unclear how the molecular mechanisms underlying STSP and exocytotic-endocytotic release are integrated (18).

The present study proposes a semiphenomenological multiple-time-scale model to explain the three modes of release as well as STSP in a unified framework. The model is derived via mass action laws and is based on the biological parsimonious view point pioneered, in particular, by Thomas Südhof (19) (a summary of the key points of the hypothesized biological model and the detailed derivations of the mathematical equations, which rests upon the assumptions of the biological model, is provided in *SI Appendix*). The resulting multiple-time-scale mathematical model describes the canonical SNARE and SM protein interaction exocytotic cycle at a mesoscopic scale, and therefore bridges the gap between molecular protein interactions and electrical synaptic activity, as observed in synaptic dual whole-cell recordings.

Significance

Neurotransmitter exocytosis and short-term synaptic plasticity (STSP) regulate large-scale brain electrical activity. This study is the first, to our knowledge, proposing a multiple-time-scale model that bridges between the microscopic and mesoscopic scales. It is parsimonious, yet with enough descriptive power to express, on the one hand, the interactions between the SNARE and Sec1/Munc18 (SM) protein complexes mediating all forms of neurotransmitter release and STSP and, on the other hand, the electrical activity required for neuronal communication. A key finding is the discovery of a mathematical structure, termed activity-induced transcritical canard, which quantifies and explains delayed and irregular exocytosis. This structure also provides a previously unidentified way to understand delayed and irregular processes sensitive to initial conditions across various biology processes.

Author contributions: S.R., M.D., M.K., T.J.S., and A.B.A. designed research; S.R., M.D., M.K., and A.B.A. performed research; S.R., M.D., M.K., J.M.C., T.J.S., and A.B.A. analyzed data; and S.R., M.D., M.K., J.M.C., T.J.S., and A.B.A. wrote the paper.

Reviewers: A.G., Universitat Politècnica de Catalunya; and M.T., Weizmann Institute of Science.

The authors declare no conflict of interest.

[1]S.R., M.D., M.K., and A.B.A. contributed equally to this work.

[2]To whom correspondence should be addressed. Email: terry@salk.edu.

This article contains supporting information online at www.pnas.org/lookup/suppl/doi:10.1073/pnas.1525591113/-/DCSupplemental.

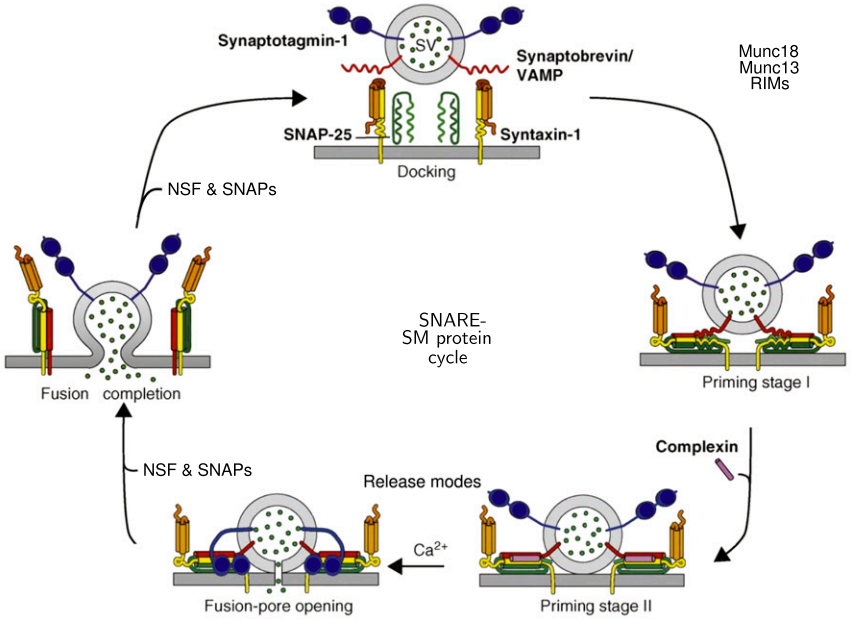

Fig. 1. Parsimonious SNARE-SM molecular exocytotic machinery (modified from ref. 1). Synaptic vesicles, docked at the active zone of a presynaptic terminal, are primed for release by partial SNARE complex assembly that is catalyzed by Munc18, Munc13, and RIMs (*Top*). The second stage involves "superpriming" due to the regulation of complexins on the assembled SNARE complexes, which gives rise to priming stage II. The primed vesicle forms a substrate for either calcium-triggered release via mediation of a calcium sensor, such as synaptotagmins, or spontaneous release, which then enables fusion-pore opening and neurotransmitter release. Subsequently, *N*-ethyl-maleimide–sensitive factor (NSF) and SNAPs mediate disassembly of the SNARE complex, leading to vesicle recycling.

SNARE-SM Model Assembly

To circumvent the prohibitive complexity of modeling all proteins and detailed (as well as unknown) protein interactions involved in the exocytotic process, we propose to model the interaction of protein complexes semiphenomenologically via first principles of mass action, that is, from a mesoscopic view point. In addition, in an attempt to reduce the time complexity of the physiological processes, the model is based on principles from nonlinear dynamics and multiple-time-scale dynamical systems theory (20–23). This approach results in a deterministic 2D model, with variables (p_1, p_2) describing the interactions between the canonical SNARE and SM protein complexes; hence, the name SNARE-SM model (*SI Appendix*). The remaining known exocytotic proteins are considered as regulatory processes, and therefore are treated as parameters that can be tuned to obtain the different modes of release, as idealized in Fig. 2.

There are numerous regulatory proteins; however, only certain proteins are expressed at any given type of synapse (e.g., in Fig. 2, VAMP4 and Syt7 may not be expressed simultaneously). This diversity suggests lumping certain proteins into a single mesoscopic parameter. In contrast, proteins that are shared between different release modes (e.g., Syt1, Syt2, complexin, RIMs, Doc2, TRPV1, voltage-gated Ca^{2+} channel) remain ungrouped. Altogether, nine parameters are associated with the regulatory proteins (model derivation for further biophysical interpretation of the model's parameters is provided in *SI Appendix*).

An important regulatory parameter is the positive small parameter $0 < \varepsilon \ll 1$, which induces a separation of time scales between p_1 and p_2. Specifically, p_1 corresponds to a slow-acting protein complex, whereas p_2 is a fast-acting protein complex. The remaining parameters regulate the interaction strength between p_1 and p_2 as well as the conformational changes of the individual protein complexes. The resulting model expresses features of slow, evoked irregular and spontaneous activation. These features emerge from the rules of interaction between the protein complexes (p_1, p_2) as expressed by the right-hand side of the SNARE-SM model equations (*SI Appendix*). These interactions are best described (in mathematical terms) by plotting the components of the interaction rules (technically, nullclines) in a 2D space (phase-space) spanned by the actions of p_1 and p_2 (Fig. 3*A* and

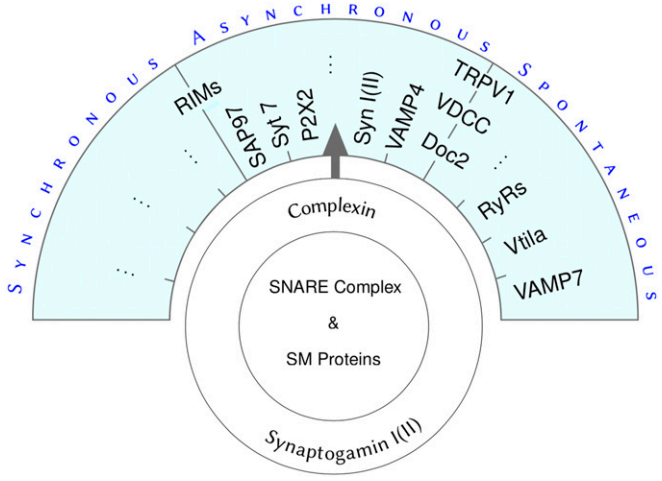

Fig. 2. Schematic idealization of the SNARE-SM model. The circular center describes the canonical fusion machinery constituted by the SNARE complex and SM proteins, which is ultimately regulated by complexin and synaptogamins (19). This building block is signaled by various proteins and, depending on the proteins involved, the appropriate neurotransmitter release mode is activated (i.e., synchronous, asynchronous, spontaneous). Some of the known proteins associated with each type of release are indicated (reviewed in 17, including a complete description and the latest view on the association between proteins and release modes). The RIM proteins are shared between synchronous and asynchronous release modes, whereas TRPV1, Doc2, and voltage-gated Ca^{2+} channels (VDCCs) are shared between asynchronous and spontaneous release modes. The remaining proteins are specific to each release mode; however, inhibiting a protein specific to a given release mode will favor the expression of other modes (17).

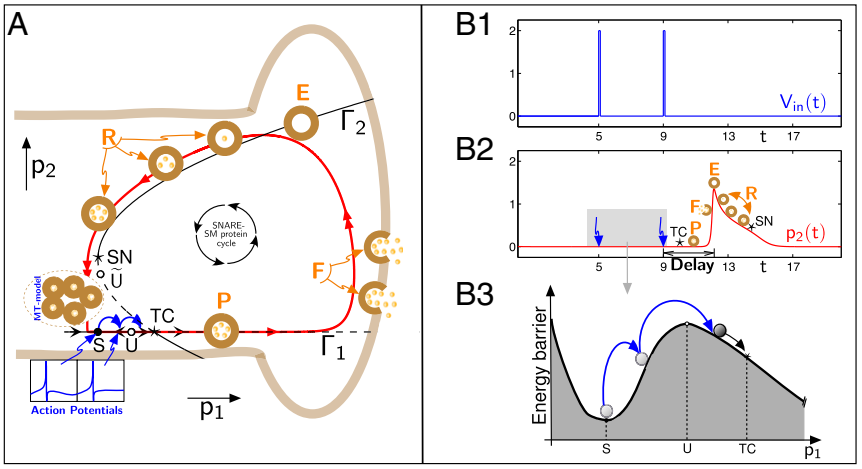

Fig. 3. SNARE-SM model dynamics and asynchronous mechanism. (*A*) Interactions between protein complexes p_1 and p_2 along the vesicle cycle are given by the parabola and the horizontal line (black). These interactions give rise to special points S, U, TC, and SN, which mediate all of the functions associated with the exocytotic-endocytotic cycle (red curve): priming (P), fusion (F), endocytosis (E), and refilling (R). Note that priming stage I initiates after point U, whereas priming stage II initiates after point TC. Arrows indicate dynamic trajectories in the phase plane. Time course of presynaptic voltage (*B1*) and p_2 activity following a stimulus (*B2*). Note that, here, *t* refers to a dimensionless time. (*B3*) Schematic diagram of an energy landscape where stimulus spikes are required to activate p_1 and p_2, represented as a particle that initiates movement only if sufficient energy is provided to traverse the energy barrier (U).

SI Appendix, Fig. S1*C*). In particular, the interaction between p_1 and p_2 gives rise to special configuration points of the dynamical system, namely, S (stable equilibrium), U (unstable equilibrium of saddle type), SN (saddle-node point), and TC (transcritical point) (Fig. 3*A* and *SI Appendix*, Fig. S1*C*), which generate all of the functions associated with each stage of the exocytosis-endocytosis cycle.

In particular, S can be associated with Munc13-1, forming a homodimer that inhibits priming. Then, U can be related to the action of Munc13 gating the transition from the closed-syntaxin/Munc18 complex to the SNARE complex formation. Subsequently, TC can be linked to the action of complexin, and, finally, SN can be connected to the refilling of the vesicle pool. It is noteworthy to observe that the resulting phase-space geometry of the mathematical model shares a great deal of similarity with the schematic diagram of the SNARE-SM biological model by Südhof (19) (compare Fig. 3*A* and *SI Appendix*, Fig. S1*C* with *SI Appendix*, Fig. S1*A*). Moreover, the model variables can be activated by a presynaptic stimulus (e.g., calcium influx), represented by the variable $V_{in}(t)$. By means of control parameters, the three modes of neurotransmitter release are mathematically translated into the model's dynamic repertoire: excitability, delayed response to input stimuli, or limit-cycle dynamics (*SI Appendix*). Importantly, the SNARE-SM model is sensitive to initial conditions without generating chaos. This sensitivity constitutes the core mechanism that governs the irregular activation. Furthermore, due to the time scale separation between p_1 and p_2, the delayed neurotransmitter release results from the protein–protein binding and subsequent unbinding that occurs with inertia.

The delay is specifically explained by a previously unexplored mathematical structure that acts as a dynamic (delayed) response to an input via transcritical canards (22, 23), which we denote, "activity-induced transcritical canards" (*SI Appendix*). This structure quantifies the delay and predicts a delayed inertial protein unbinding associated with the SNARE complex assembly immediately after vesicle priming. Previous modeling attempts introduced stochastic elements or a hardwired delay into the model to account for asynchronous release (24–28). In contrast, the delay in the SNARE-SM model emerges as a result of a dynamic mechanism that resembles a biological process.

In brief, the SNARE-SM model has a mechanistic interpretation because it can be related to processes associated with exocytotic-endocytotic signaling pathways, including intracellular calcium dynamics. Moreover, the delayed irregular activation can be associated, for example, with the action of complexin or Syn I(II) and with the presence of eCB, VAMP4, or even Doc2 in the case of excitatory neurons.

Extended SNARE-SM Model. We extend the SNARE-SM model to show how STSP mechanistically integrates within the exocytotic-endocytotic machinery, and also to enable comparison with electrophysiological data. This extension is achieved by feeding the exocytotic-endocytotic signal of the SNARE-SM model into an STSP model, which effectively activates the vesicle pool. In particular, we use the Markram–Tsodyks (MT) STSP model (29–31) (*SI Appendix*). The MT equations phenomenologically model the time evolution of available resources (vesicles) and how efficiently neurotransmitters are released. In the model there are two quantities, namely, the number of vesicles, d, and the release probability, f, which are updated for every presynaptic spike occurring at time instant t_s. The model predicts the amount of neurotransmitter released, $T(t_s) = d(t_s)f(t_s)$, which, in reality, is released with a small time delay.

The MT model successfully accounts for the highly heterogeneous STSP dynamics across different brain areas in the context of synchronous release (table S1 of ref. 31). Consequently, the proposed model extends the MT model by incorporating all three modes of neurotransmitter release observed at unitary synapses. However, to complete the model framework and to enable testing against data sampled from whole-cell paired recordings obtained from unitary synapses, an observational variable representing postsynaptic potentials is required. This observational variable is modeled with the standard conductance-based (subthreshold) equation, where the action of neurotransmitters on postsynaptic neurotransmitter receptors follows the first-order kinetic equation (*SI Appendix*). More detailed approaches for modeling receptor dynamics [e.g., detailed kinetics (32)] will be a matter for future consideration.

Results

SNARE-SM Model Dynamics. The SNARE-SM model has three operating modes. Fig. 3*A* shows a presynaptic terminal, which encloses the SNARE-SM model's signaling mechanism. The black arrows labeled p_1 and p_2 span the 2D space within which the protein complexes interact. This space is not physical, but

rather a phase-space where protein functions take place and the values of p_1 and p_2 represent the levels of activity between protein complexes. The line Γ_1 and the parabola Γ_2, called the fast nullclines, indicate the regions in which the functions of the protein complexes are quasistationary (Fig. 3*A* and *SI Appendix*, Fig. S1*C*). The line Γ_1 is stable to the left of the transition point TC, and the parabola Γ_2 is stable above the transition point SN. Past the transition points, the fast nullclines become unstable (Fig. 3*A* and *SI Appendix*, Fig. S1*C*, dashed lines). For clarity, the slow nullclines are not displayed (*SI Appendix*).

The stability of the fast nullclines is assessed by looking at the mathematical limit of the model when p_1 is kept constant ($\varepsilon = 0$) (details are provided in *SI Appendix*). In this limit, the only variable left is p_2, and p_1 acts as a parameter; the equilibrium states lie on the fast nullclines, and their stability depends on the parameter p_1 and change at bifurcation points SN and TC. Under normal operating conditions ($\varepsilon > 0$), p_1 evolves slowly; the points SN and TC are not bifurcation points of the model any longer; however, they still organize dynamic transitions between different levels of quasistationary activity close to Γ_1 and Γ_2. Moreover, the SNARE-SM model possesses two true stationary states, marked S and U (Fig. 3*A* and *SI Appendix*, Fig. S1*C*), which endow it with an excitable structure.

An exocytotic signal (Fig. 3*A*, red trajectory) is evoked by one or more presynaptic spikes. Input stimuli excite the system away from the functionally inactive state S. However, the protein complexes switch their functional behavior past the switching point (U) only when sufficient energy is available, via action potentials and an increase in calcium influx. In this case, the system passes the TC transition point, which enables the appropriate exocytotic signaling mode to be activated. Fig. 3*B* illustrates the process in the time domain: Fig. 3*B1* shows the presynaptic stimulus; Fig. 3*B2* shows the output signal; and Fig. 3*B3* is a schematic diagram that depicts a particle (in the abstract sense), initially at a rest point (S), that is driven out of the basin of attraction of S by a sufficient force (blue arrows), enabling it to jump the energy barrier (U). We refer the reader to the article by Kasai et al. (33) for discussion on energy functions associated with the release of neurotransmitters. Thus, a particular amplitude and timing of a perturbation can drive the system away from the equilibrium point and induce it to make a large-amplitude, transient excursion before it settles again to its inactive state (S).

Past the switching point (U), the protein complexes p_1 and p_2 begin to interact strongly, activating states associated with vesicle priming I. The passage through the TC point can be associated with the initiation of priming stage II (i.e., SNARE complex assembly and regulation by complexin). Priming can be a fast (synchronous) or slow (asynchronous) process, depending on the time scale parameter ε.

From a mathematical perspective, precise quantitative control of the delay is achieved by the so-called "way-in–way-out function" (*SI Appendix*). In short, the activity-induced transcritical canard predicts the existence of delayed inertial protein unbinding occurring between priming I and fusion-pore opening stages. This delayed inertial protein unbinding can possibly be related to the clamping action of complexin, or Ca^{2+}-activated calcium sensors (e.g., Syt1) competing with complexin for SNARE complex binding (by displacing part of complexin within the SNARE but via a delayed inertial unbinding). Indeed, from the modeling point of view, ε (which also controls the delayed process), can be associated with complexin or (a)synchronous calcium sensors at a molecular level (*SI Appendix*). The unbinding between p_1 and p_2 (e.g., interpreted mesoscopically as translocation of complexin) initiates fusion (F) and subsequent neurotransmitter release. Following exocytosis, p_1 and p_2 begin a second phase of strong interaction that induces endocytosis (E) and subsequent vesicle refilling (R). The final stage is triggered by the SN transition point, which prompts p_1 and p_2 to alter their states and evolve toward their inactive state S, where the vesicle pool is replenished.

SNARE-SM Model Evoked Release Mode. Evoked synchronous and asynchronous modes of release in the SNARE-SM model are shown in *SI Appendix*, Figs. S2 and S3, with the parameters specified in *SI Appendix*, Table S1. For the synchronous mode, *SI Appendix*, Fig. S3 *A–A2* shows that the SNARE-SM model's output, p_2, is activated almost instantaneously upon an incoming stimulus, V_{in}. In this case, ε has a small value. Increasing ε induces a weaker binding/unbinding that effectively introduces variability (irregular activation via sensitivity to initial conditions) and a strong inertia in the unbinding process, causing a delay. This asynchronous mode is shown in *SI Appendix*, Fig. S3 *B–B2*, where the onset of p_2 is delayed with respect to the stimulus. Note that the output time profile also changes shape and amplitude, with a slower rising phase. These features are crucial, leading to gradual activation of vesicle pools as well as postsynaptic receptors, consistent with the gradual postsynaptic potential response observed in experiments for asynchronous release (1).

SI Appendix, Fig. S2 shows three different delayed responses under the same two-spike stimulus, demonstrating irregular activation due to the model's sensitivity to initial conditions. Moreover, a burst of spikes may be required before the vesicle pool is activated, a feature that is widely reported in experiments (1); this burst of spikes is controlled by increasing the distance between the two configuration states S and U, thereby increasing the energy barrier (Fig. 3*B3*). The farther they are apart, the stronger is the stimulus (multiple spikes) that is needed to elicit vesicle priming (P). A delayed response to a stimulus with three spikes is shown in *SI Appendix*, Fig. S3 *C–C2*). Note that if the interspike interval between input stimuli is smaller than the exocytotic-endocytotic cycle time, then the delay decreases inversely to the input frequency increase. However, this delay does not decrease below a fixed value that corresponds to synchronous release.

SNARE-SM Model Spontaneous Release Mode. There are two different ways to generate spontaneous mini-releases in the SNARE-SM model as illustrated in *SI Appendix*, Fig. S4 *A–B1*, respectively. One way is to assume that Ca^{2+} channels open stochastically, which changes the resting baseline of Ca^{2+} concentrations (2). Increasing the Ca^{2+} concentration decreases the amplitude of the parabola Γ_2, which changes the fusion dynamics. This change can be related to empirical data showing the existence of multiple fusion processes, such as kiss-and-run, clathrin-dependent endocytosis, and bulk endocytosis (34). Kiss-and-run is relevant to spontaneous release, where vesicles do not fuse entirely with the membrane, and thus are rapidly retrieved from the active zone (release site).

The model also needs to be in a strongly excitable regime, in which the two configuration states S and U are sufficiently close to each other. As a consequence, low-noise perturbations are sufficient to kick the system away from its inactive state (S) to complete endocytosis before settling back to S (*SI Appendix*, Fig. S4*B1*). An alternative mode of spontaneous release is via Ca^{2+} sparks from internal Ca^{2+} stores (1, 2), which stimulates a limit cycle (a self-sustained periodic signal) (*SI Appendix*, Fig. S4*A1*) that is achieved by moving both the S and U configuration points to the far left; as a consequence, signals emanating from the SN point no longer fall into the basin of attraction of S, prompting another exocytotic-endocytotic cycle. The limit cycle can have an irregular period by random variation of its associated parameters (*SI Appendix*).

Extended SNARE-SM Model Predictions. We now test the full model [extended (E)-SNARE-SM] with paired whole-cell recordings from both inhibitory and excitatory synapses having differential modes of exocytosis. For inhibition, we use recordings from isolated synapses between cholecystokinin (CCK)-positive Shaffer collateral-associated

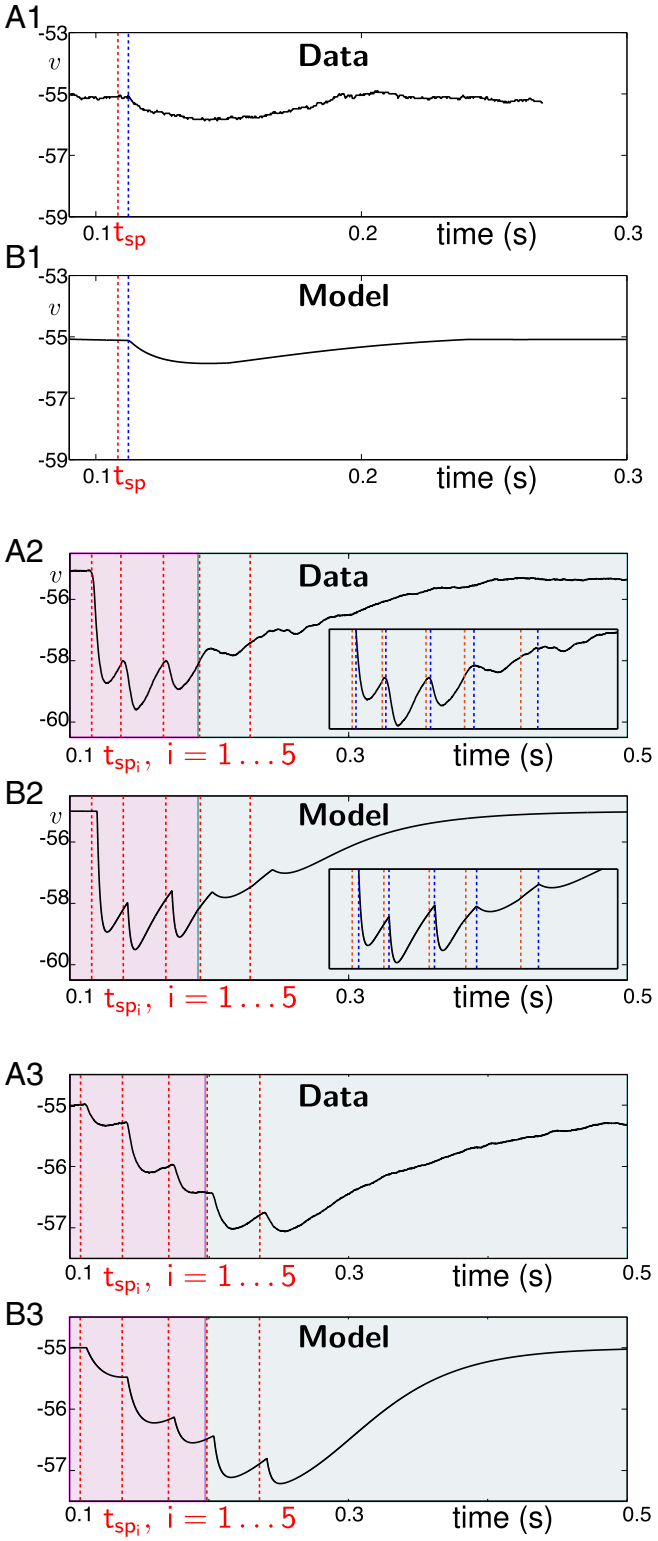

Fig. 4. Model comparison with inhibitory synapse. (*A1*) Delayed IPSP (~5.6 ms) of CCK-positive SCA interneuron to unitary input spike at time t_{sp} (dashed red line). (*B1*) Response of the model to the same input as in *A1*. (*A2*) Depressed and delayed IPSP data resulting from spikes occurring at times t_{sp_i}, $i = \{1 \ldots 5\}$ (red dashed lines). The first epoch (shaded magenta rectangle) is triggered by the first three spikes causing synchronous mode (release within 5 ms); the second epoch (shaded cyan rectangle) is initiated by two subsequent spikes that lead to asynchronous mode (more than 5-ms delayed release). (*Inset*) Expansion of the region corresponding to the five release events: Vertical red dashed lines mark spike times, and vertical blue lines mark IPSP response times. The distance between them measures the delay: ~(2.0, 2.6, 2.5, 9.2, 15.0) ms. (*B2*) Response of the model to the same input as in *A2*. (*A3*) Facilitated and delayed IPSP data. The first epoch (shaded magenta rectangle), induced by the first three spikes, leads to synchronous release with delayed response times of ~(4.2, 3.6, 4.1) ms. The second epoch (shaded cyan rectangle) is evoked by two subsequent spikes, with marginal delayed release times [~(5.0, 5.1) ms]. (*B3*) Response of the model to the same input as in *A3*.

(SCA) interneurons in the CA1 region of P18-21 rat hippocampus (16) (*Materials and Methods*) and we base the model on parameters associated with $GABA_A$-induced currents (16, 35, 36). For excitation, we use data from experiments on calyx-of-Held synapses (4). The SNARE-SM model parameters are adjusted to generate the appropriate release mode (*SI Appendix*, Table S1), and the MT model parameters are adopted from Markram et al. (37) as a baseline (*SI Appendix*). Note that asynchronous release is known to be accompanied by irregularity in both neurotransmitter release times and amplitudes of the inhibitory postsynaptic potentials (IPSPs) and excitatory postsynaptic potentials; therefore, associated parameter values can vary substantially between release events. The remaining parameters are tuned within a bounded region (inhibitory synapses are shown in *SI Appendix*, Table S2, and excitatory synapses are shown in *SI Appendix*, Table S3). Details of the parameter fitting procedures are provided in *SI Appendix*.

The E-SNARE-SM model successfully reproduces the synaptic dynamics of the SCA inhibitory synapse (Fig. 4). The delayed unitary IPSP in Fig. 4*A1* is compared with the output of the inhibitory model (Fig. 4*B1*). A sequence of IPSPs exhibiting short-term synaptic depression and delay in response to multiple presynaptic stimuli (Fig. 4*A2*) matches the output of the model in Fig. 4*B2*. The response to a sequence of IPSPs featuring short-term synaptic facilitation and delay, shown in Fig. 4*A3*, is compared with the response of the model in Fig. 4*B3*. The model reproduces the onset of the delays and the temporal profile of the IPSP data. Care was taken with fitting delayed release because the model is sensitive to initial conditions. Completion of an exocytotic-endocytotic cycle brings the system to a different configuration. As a consequence, the parameters of the previous exocytotic-endocytotic cycle will give rise to a different delayed response when a new stimulus occurs. Parameters associated with $GABA_A$-induced currents also undergo changes, albeit minor, because eCBs increase the input resistance of the cell, docking time of neurotransmitters, and affinity.

The parameters of the MT model also depend on the mode of release. Continuity conditions are enforced to ensure that different epochs of data fit with different modes of release (shaded magenta and cyan rectangles in Fig. 4 *A2*, *B2*, *A3*, and *B3*). Future developments will include the conditions ensured by the way-in–way-out function for an automatic parameter fitting. However, in the limit of complete depletion of neurotransmitters, fitting any continuous mesoscopic model to electrophysiological data becomes increasingly difficult, because noise dominates and expressing microscopic dynamics becomes fundamental (averaging effect is shown in *SI Appendix*, Fig. S7). In this limit, other theoretical studies reveal that discrete, stochastic, or agent-based models best describe microscopic activity (38).

Comparisons between excitatory postsynaptic currents at the calyx-of-Held synapse and the postsynaptic currents of the E-SNARE-SM model are made in Fig. 5. Specifically, Fig. 5*A1* depicts a synchronous activation to a single presynaptic spike, which is matched by the model in Fig. 5*B1*. Multiple postsynaptic activations elicited by a single input are shown in Fig. 5*A2*. The first postsynaptic activation is asynchronous, and the two subsequent releases are spontaneous. The model is in good agreement over three epochs shown in different colors (Fig. 5*B2*). Moreover, the model can also reproduce the WT data from the calyx of Held.

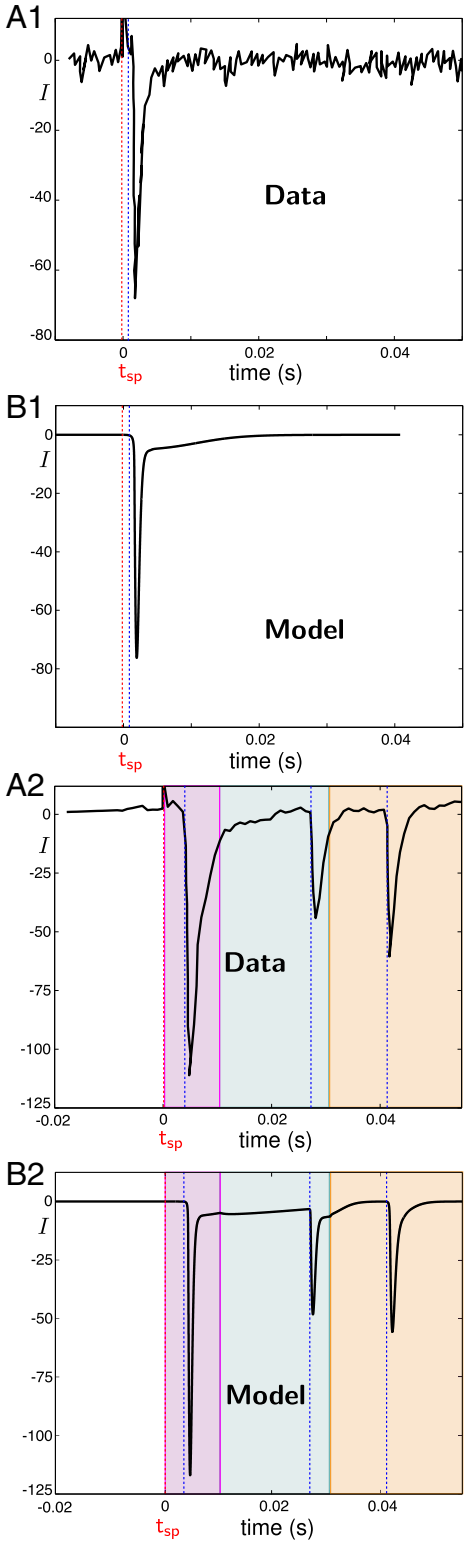

Fig. 5. Model comparison with excitatory synapse. (*A1*) Synchronous excitatory postsynaptic current (EPSC; at ∼1.6 ms) of the calyx-of-Held synapse to unitary input spike at time t_{sp} (dashed red line). The blue dashed line shows the time instant of activation. Data were extracted from figure 2A of ref. 4 (Syt2 KO). (*B1*) Response of the model to the same input as in *A1*. (*A2*) Unitary input spike at time t_{sp} (dashed red line) first causes a delayed EPSC (at ∼4 ms) and two additional spontaneous activations at ∼(27.3, 41.3) ms. Data were extracted from figure 2A of ref. (4) (Syt2 KO). (*B2*) Response of the model to the same input as in *A2*. Here, the different epochs of the data reflect the transitions from delayed (shaded magenta rectangle) to spontaneous (shaded cyan and shaded light orange rectangles) activation. The model makes these transitions by varying the parameters of the SNARE-SM model that dictate the transition from the delayed to spontaneous regime (*SI Appendix*, Table S1).

In particular, the strong synaptic depression seen at this synapse during high-frequency stimulation and the kinetics of recovery from synaptic depression can both be captured. Indeed, our model builds upon the MT framework, which has been shown to account for these phenomena (39).

Discussion

The proposed multiple-time-scale SNARE-SM model extends the MT framework for STSP by incorporating all three forms of exocytosis at the same mesoscopic level of description (37). Moreover, our mathematical model is in good agreement with the biological SNARE-SM model of Südhof (19) (compare again Fig. 3 and *SI Appendix*, Fig. S1*C* with *SI Appendix*, Fig. S1*A*). Details of the biochemical pathways involved in exocytosis are semiphenomenologically expressed; therefore, predictions of the model can be compared with SNARE-SM physiology, and computational hypotheses can be explored to propose novel experiments. For example, in the model, the three distinct forms of release share the same exocytotic machinery, where the modes of exocytosis are a consequence of parameters in the model. Therefore, in every exocytosis-endocytosis cycle, the release mode may switch due to slowly varying physiological variables that have not yet been identified. However, it is important to be cautious because there may be different vesicle pools or pathways (e.g., different calcium sensors) (4).

The time-scale parameter ε modulates the activity-induced transcritical canard, which mechanistically explains the ratio between synchronous and asynchronous release. The way-in–way-out function quantifies how the exocytotic-endocytotic signaling pathway fine-tunes the timing of neurotransmitter release, which can be seen as a homeostatic mechanism for efficient neuronal communication. This mechanism is consistent with molecular studies showing that within the canonical fusion machinery, Syt1 and complexin are functionally interdependent and are potentially the key players in regulating all modes of release (19). Specifically, Syt1 mediates calcium-triggered release and controls the rate of spontaneous release (i.e., speed and precision of release by associations with SNARE complexes). Complexin is a cofactor for Syt1 that functions both as a clamp and as an activator of calcium-triggered fusion (19).

Further upstream, other proteins could signal (via yet unknown interactions) this homeostatic system. For example, studies show that Syn I(II), known to coat synaptic vesicles and to have a postdocking role, regulates synchronous and asynchronous release (15). In particular, Syn II interacts directly with P/Q type and indirectly with N-type Ca^{2+} channels to increase asynchronous release. Additionally, Syn I(II) seems to constitute a push/pull mechanism regulating the ratio between synchronous and asynchronous release (15), thus suggesting that they share exocytotic mechanisms. Deeper insight into this mechanism could result from further molecular studies investigating the existence of a signaling pathway between cannabinoid type 1 (CB1) receptor, Syn I(II), RIMs, and RIM-BS proteins, because CB1 also appears to interact with N-type and P/Q-type Ca^{2+} channels (40, 41). Nevertheless, multiple exocytotic mechanisms should not be ruled out, and augmenting the proposed model to allow switching between them is a focus for future research.

The proposed model could also be mapped onto the dual calcium-sensor model (4). Another reported mechanism that should be considered is the VAMP4-enriched vesicle pool, which

is formed after intense stimulation and enables asynchronous release (11). Surprisingly, the authors show that VAMP4-driven SNARE complexes do not readily interact with synaptotagmin and complexin, which challenges the widely held view that synchronous release requires interaction of SNARE complexes (e.g., VAMP4/SNAP-25, syntaxin-1) with Syt1 and complexins. This issue could be resolved by seeking an alternative way to elicit VAMP4-mediated release (identifying a different signaling pathway). In view of the present model, it would be relevant to test for VAMP4 in synapses expressing CCK. Despite these observations, the SNARE-SM model can explain these results without assuming the existence of a second, VAMP4-enriched pool of vesicles (*SI Appendix*, Fig. S5 *B–B2*). Another refinement may emerge from a recent study showing that 2-arachidonoyglycerol (2-AG)/anandamide directly modulates $GABA_A$ postsynaptic receptors, therefore affecting neurotransmitter docking times and possibly contributing to asynchronicity (42). Other forms of synaptic plasticity, such as spike timing-dependent plasticity mediated by differential exocytosis, could also be explored with the proposed model (*SI Appendix*, Fig. S6).

Finally, the SNARE-SM model will facilitate large-scale network simulations and consequently explain the functional role of differential exocytosis and synaptic plasticity on network states underlying memory, cognition, and pathological brain states (e.g., epilepsy) (43). At a microscale, the proposed theoretical approach could provide new insights into the function of other protein–protein interactions. For example, activity-induced transcritical canards can explain recent experiments that identify proteins mediating the asynchronous activation of sodium and potassium channels (44).

Materials and Methods

Inhibitory Synapses.

Experimental preparations and observations. The data are sampled from paired whole-cell recordings obtained from unitary synapses between CCK-positive SCA interneurons in the CA1 region of P18–P21 rat hippocampus (45) (*SI Appendix*, Fig. S7). These cells possess a modulatory feedback mechanism that allows the postsynaptic cell to control the level of presynaptic $GABA_A$ release via the eCB system, which is composed of cannabinoid receptors, ligands, and the relevant enzymes (45). Specifically, eCB, 2-AG, or anandamide is synthesized and released on demand, involving depolarization of the postsynaptic membrane via the activation of voltage-dependent L-type calcium channels (46). Once synthesized, it diffuses across the synaptic cleft to modulate the activation of CB1 receptors located in the presynaptic cell. Subsequently, CB1 receptors inactivate N-type (and possibly P/Q-type) calcium channels (therefore reducing Ca^{2+} concentration) leading to a reduction of $GABA_A$ release (45). Experimentally, the level of CB1 receptor activation and deactivation was controlled by bath application of endogenous agonist, anandamide, and antagonist AM-251. The endogenous agonist effects could be mimicked by depolarization-induced suppression of inhibition protocols, which involved depolarization of the postsynaptic membrane (45). These modulatory synaptic effects have a direct impact on the timing of synaptic inhibition, specifically asynchronous release and STSP (*SI Appendix*, Fig. S7). Details of the experimental preparation are explained.

Slice preparation. Male Wistar rats (P18–P23; Harlan UK) were anesthetized with sodium pentobarbitone (60 mg/kg Euthatal; Merial) via i.p. injection and perfused transcardially with ice-cold modified artificial cerebral spinal fluid (ACSF) containing 15 mM D-glucose, 248 mM sucrose, 2.5 mM $CaCl_2$, 3.3 mM KCl, 1.2 mM $MgCl_2$, 25.5 mM $NaHCO_3$, and 1.4 mM NaH_2PO_4. Following decapitation, the brain was removed and 300-μm-thick coronal slices of cerebral cortex were cut. These procedures were performed under UK Home Office guidelines by authorized Home Office license holders. The severity of the procedures was classed as moderate. The total number of rats used for this study was 61. Slices were incubated for 1 h before recording, for which they were placed in a submerged chamber perfused with ACSF at a rate of 1–2 $mL \cdot min^{-1}$. ACSF contained 20 mM D-glucose, 2 mM $CaCl_2$, 2.5 mM KCl, 1 mM $MgCl_2$, 121 mM NaCl, 26 mM $NaHCO_3$, and 1.25 mM NaH_2PO_4 [equilibrated with 95% (vol/vol) O_2 and 5% (vol/vol) CO_2]. All substances used to make ACSF solutions were obtained from VWR International (45).

Electrophysiological recordings. Electrodes with resistances of 8–11 MΩ were pulled from borosilicate glass and filled with an intracellular solution containing 144 mM K-gluconate, 0.2 mM EGTA, 10 mM Hepes, 3 mM $MgCl_2$, 0.2 mM Na_2-ATP, 0.2 mM Na_2-GTP, and 0.02% (wt/vol) biocytin (pH 7.2–7.4, 300 mOsm). Slices were viewed using videomicroscopy under near-differential interference contrast illumination to enable cells to be chosen based upon the shape of their soma and dendritic projections. Neurons were further identified by their firing properties following a series of 500-ms depolarizing current steps from +0.05 nA to +0.15 nA. Dual whole-cell recordings were performed in a current clamp at room temperature in CA1 stratum radiatum and lacunosum moleculare border. Presynaptic action potentials were generated by a depolarizing current injection of varying length (5–10 ms) to enable IPSPs to be observed in response to single, double, or trains of action potentials. Connections were tested in both directions for all pairs. Data were acquired with SEC 05L/H amplifiers (NPI Electronic GmbH). Recordings were filtered at 2 KHz, digitized at 5 KHz using a CED 1401 interface (Cambridge Electronic Design), and stored on a hard disk drive. Input resistances were continually monitored by injecting a small hyperpolarizing current injection for 20 ms at the start of each frame.

Pharmacology. The endogenous cannabinoid receptor agonist anandamide (14 μM, in water-soluble emulsion) was used. AM-251 [1-(2,4-dichlorophenyl)-5-(4-iodophenyl)-4-methyl-*N*-(1-piperidyl)pyrazole-3-carboxamid; Tocris], a selective CB1 receptor inverse agonist, was dissolved in DMSO, stored as stock at −20 °C, and bath-applied at 10 μM. AM-251 is structurally very close to SR141716A, a cannabinoid receptor antagonist, but it exhibits a higher binding affinity for the CB1 receptor with a K_i value of 7.5 nM compound to SR141716A, which has a K_i value of 11.5 nM.

Electrophysiological data analysis. Using Signal (Cambridge Electronic Design), the electrophysiological characteristics of the recorded cells were measured from their voltage responses to 500-ms current pulses between −0.2 and +0.1 nA in amplitude. Postsynaptic events were either accepted for analysis or rejected. Individual sweeps were observed and accepted, edited, or rejected according to the trigger points that would trigger measurements and averaging of the IPSPs during subsequent data analysis. Averaging of IPSPs was triggered from the rising phase of the presynaptic spike. Apparent failures of synaptic transmission were counted manually, and IPSP amplitudes in the range of the synaptic noise were taken as failures. Selection and averaging of these apparent failures resulted in no measurable postsynaptic responses. Single-sweep IPSP amplitudes were measured from the baseline to the peak of the IPSP and are displayed as ±SD. IPSP half-width and the 10–90% rise time were obtained from averages created from 100 to 300 sweeps. IPSP latencies were manually measured as the time delay between presynaptic action potential peaks to the onset of the detectable IPSPs. The fluctuations in the IPSP latencies were quantified in nonoverlapping time interval sets of 5 ms after each presynaptic action potential. Synchronous release was taken as release of neurotransmitter within 0- to 5-ms latencies, whereas asynchronous release was taken as the release of neurotransmitter falling within a time window of 5- to 15-ms latencies (40). The synchronicity ratio was calculated as the ratio of synchronous release/asynchronous release (from a dataset of 100–300 sweeps).

Excitatory Synapses. Recordings were performed in the laboratory of Thomas Südhof (Stanford University, Stanford, CA). In particular, data in Fig. 4 *A1* and *A2* were extracted from figure 2A of ref. 10 (Syt2 KO).

Software. Electrophysiological data were acquired and analyzed offline using Signal. For model simulations, we used the software package XPPAUT (47). The parameter fitting of the model from data was carried out with MATLAB (MathWorks).

ACKNOWLEDGMENTS. We thank Dr. Thomas Südhof (Stanford University) for providing voltage-clamp recordings of the calyx-of-Held synapses (4). A.B.A. thanks the Medical Research Council (United Kingdom) New Investigators Award for funding the experiments. J.M.C. is funded by Ikerbasque: The Basque Foundation for Science. T.J.S. is supported by the Howard Hughes Medical Institute, NIH, and Office of Naval Research.

1. Pang ZP, Südhof TC (2010) Cell biology of Ca2+-triggered exocytosis. *Curr Opin Cell Biol* 22(4):496–505.
2. Smith SM, et al. (2012) Calcium regulation of spontaneous and asynchronous neurotransmitter release. *Cell Calcium* 52(3):226–233.
3. Sara Y, Virmani T, Deák F, Liu X, Kavalali ET (2005) An isolated pool of vesicles recycles at rest and drives spontaneous neurotransmission. *Neuron* 45(4):563–573.
4. Sun J, et al. (2007) A dual-Ca2+-sensor model for neurotransmitter release in a central synapse. *Nature* 450(7170):676–682.

5. Verhage M, et al. (2000) Synaptic assembly of the brain in the absence of neurotransmitter secretion. *Science* 287(5454):864–869.
6. Schoch S, et al. (2001) SNARE function analyzed in synaptobrevin/VAMP knockout mice. *Science* 294(5544):1117–1122.
7. Bronk P, et al. (2007) Differential effects of SNAP-25 deletion on Ca2+ -dependent and Ca2+ -independent neurotransmission. *J Neurophysiol* 98(2):794–806.
8. Zhou P, et al. (2013) Syntaxin-1 N-peptide and Habc-domain perform distinct essential functions in synaptic vesicle fusion. *EMBO J* 32(1):159–171.
9. Broadie K, et al. (1995) Syntaxin and synaptobrevin function downstream of vesicle docking in Drosophila. *Neuron* 15(3):663–673.
10. Vilinsky I, Stewart BA, Drummond J, Robinson I, Deitcher DL (2002) A Drosophila SNAP-25 null mutant reveals context-dependent redundancy with SNAP-24 in neurotransmission. *Genetics* 162(1):259–271.
11. Raingo J, et al. (2012) VAMP4 directs synaptic vesicles to a pool that selectively maintains asynchronous neurotransmission. *Nat Neurosci* 15(5):738–745.
12. Maximov A, et al. (2008) Genetic analysis of synaptotagmin-7 function in synaptic vesicle exocytosis. *Proc Natl Acad Sci USA* 105(10):3986–3991.
13. Pang ZP, et al. (2011) Doc2 supports spontaneous synaptic transmission by a Ca(2+)-independent mechanism. *Neuron* 70(2):244–251.
14. Calakos N, Schoch S, Südhof TC, Malenka RC (2004) Multiple roles for the active zone protein RIM1α in late stages of neurotransmitter release. *Neuron* 42(6):889–896.
15. Medrihan L, et al. (2013) Synapsin II desynchronizes neurotransmitter release at inhibitory synapses by interacting with presynaptic calcium channels. *Nat Commun* 4:1512.
16. Ali AB (2007) Presynaptic Inhibition of $GABA_A$ receptor-mediated unitary IPSPs by cannabinoid receptors at synapses between CCK-positive interneurons in rat hippocampus. *J Neurophysiol* 98(2):861–869.
17. Kaeser PS, Regehr WG (2014) Molecular mechanisms for synchronous, asynchronous, and spontaneous neurotransmitter release. *Annu Rev Physiol* 76:333–363.
18. Lipstein N, et al. (2013) Dynamic control of synaptic vesicle replenishment and short-term plasticity by Ca(2+)-calmodulin-Munc13-1 signaling. *Neuron* 79(1):82–96.
19. Südhof TC (2013) A molecular machine for neurotransmitter release: Synaptotagmin and beyond. *Nat Med* 19(10):1227–1231.
20. Krupa M, Szmolyan P (2001) Extending slow manifolds near transcritical and pitchfork singularities. *Nonlinearity* 14(6):1473–1491.
21. Desroches M, Krupa M, Rodrigues S (2013) Inflection, canards and excitability threshold in neuronal models. *J Math Biol* 67(4):989–1017.
22. Lobry C (1991) Dynamic bifurcations. *Lecture Notes in Math*, ed Benoît E (Springer, Berlin), Vol 1493, pp 1–13.
23. Benoît E, et al. (1981) Chasse au canard. *The College Mathematics Journal* 32:37–119.
24. Volman V, Gerkin RC, Lau PM, Ben-Jacob E, Bi GQ (2007) Calcium and synaptic dynamics underlying reverberatory activity in neuronal networks. *Phys Biol* 4(2):91–103.
25. Nadkarni S, Bartol TM, Sejnowski TJ, Levine H (2010) Modelling vesicular release at hippocampal synapses. *PLOS Comput Biol* 6(11):e1000983.
26. Volman V, Levine H, Sejnowski TJ (2010) Shunting inhibition controls the gain modulation mediated by asynchronous neurotransmitter release in early development. *PLOS Comput Biol* 6(11):e1000973.
27. Volman V, Gerkin RC (2011) Synaptic scaling stabilizes persistent activity driven by asynchronous neurotransmitter release. *Neural Comput* 23(4):927–957.
28. Nadkarni S, Bartol TM, Stevens CF, Sejnowski TJ, Levine H (2012) Short-term plasticity constrains spatial organization of a hippocampal presynaptic terminal. *Proc Natl Acad Sci USA* 109(36):14657–14662.
29. Markram H, Tsodyks M (1996) Redistribution of synaptic efficacy between neocortical pyramidal neurons. *Nature* 382(6594):807–810.
30. Tsodyks MV, Markram H (1997) The neural code between neocortical pyramidal neurons depends on neurotransmitter release probability. *Proc Natl Acad Sci USA* 94(2):719–723.
31. Wang Y, et al. (2006) Heterogeneity in the pyramidal network of the medial prefrontal cortex. *Nat Neurosci* 9(4):534–542.
32. Raghavachari S, Lisman JE (2004) Properties of quantal transmission at CA1 synapses. *J Neurophysiol* 92(4):2456–2467.
33. Kasai H, Takahashi N, Tokumaru H (2012) Distinct initial SNARE configurations underlying the diversity of exocytosis. *Physiol Rev* 92(4):1915–1964.
34. Danglot L, Galli T (2007) What is the function of neuronal AP-3? *Biol Cell* 99(7): 349–361.
35. Cea-del Rio CA, Lawrence JJ, Erdelyi F, Szabo G, McBain CJ (2011) Cholinergic modulation amplifies the intrinsic oscillatory properties of CA1 hippocampal cholecystokinin-positive interneurons. *J Physiol* 589(Pt 3):609–627.
36. Tricoire L, et al. (2011) A blueprint for the spatiotemporal origins of mouse hippocampal interneuron diversity. *J Neurosci* 31(30):10948–10970.
37. Markram H, Wang Y, Tsodyks M (1998) Differential signaling via the same axon of neocortical pyramidal neurons. *Proc Natl Acad Sci USA* 95(9):5323–5328.
38. Campillo F, Lobry C (2012) Effect of population size in a predator–prey model. *Ecol Modell* 246:1–10.
39. Hermann J, Grothe B, Klug A (2009) Modeling short-term synaptic plasticity at the calyx of Held using in vivo-like stimulation patterns. *J Neurophysiol* 101(1):20–30.
40. Twitchell W, Brown S, Mackie K (1997) Cannabinoids inhibit N- and P/Q-type calcium channels in cultured rat hippocampal neurons. *J Neurophysiol* 78(1):43–50.
41. Ali AB (2011) CB1 modulation of temporally distinct synaptic facilitation among local circuit interneurons mediated by N-type calcium channels in CA1. *J Neurophysiol* 105(3):1051–1062.
42. Sigel E, et al. (2011) The major central endocannabinoid directly acts at $GABA_(A)$ receptors. *Proc Natl Acad Sci USA* 108(44):18150–18155.
43. Cortes JM, et al. (2013) Short-term synaptic plasticity in the deterministic Tsodyks-Markram model leads to unpredictable network dynamics. *Proc Natl Acad Sci USA* 110(41):16610–16615.
44. Lacroix JJ, Campos FV, Frezza L, Bezanilla F (2013) Molecular bases for the asynchronous activation of sodium and potassium channels required for nerve impulse generation. *Neuron* 79(4):651–657.
45. Ali AB, Todorova M (2010) Asynchronous release of GABA via tonic cannabinoid receptor activation at identified interneuron synapses in rat CA1. *Eur J Neurosci* 31(7): 1196–1207.
46. Lenz RA, Wagner JJ, Alger BE (1998) N- and L-type calcium channel involvement in depolarization-induced suppression of inhibition in rat hippocampal CA1 cells. *J Physiol* 512(Pt 1):61–73.
47. Ermentrout B (2002) *Simulating, Analyzing, and Animating Dynamical Systems: A Guide to XPPAUT for Researchers and Students* [Society for Industrial and Applied Mathematics (SIAM), Philadelphia].